Mechanistic Studies on the Selective Reduction of CO_2 to the Aldehyde Level by a PBP-Supported Nickel Complex

Pablo Ríos, Amor Rodríguez and Joaquín López-Serrano**

Instituto de Investigaciones Químicas-Departamento de Química Inorgánica, Centro de Innovación en Química Avanzada (ORFEO-CINQA). Universidad de Sevilla-Consejo Superior de Investigaciones Científicas. Calle Américo Vespucio 49, 41092. Seville (Spain)

ABSTRACT: This work describes a thorough investigation of the mechanism of a highly selective hydrosilylation of CO_2 to the formaldehyde level catalyzed by a bis(phosphino)boryl (PBP)Ni(II) complex in the presence of $B(C_6F_5)_3$. CO_2 activation by insertion into the Ni-H bond of the catalyst precursor **2** is shown to occur very easily due to the *trans* influence exerted by the boryl ligand. During catalysis, the limiting step is $B(C_6F_5)_3$ dissociation from the active species (PBP)Ni-OCHO·$B(C_5F_6)_3$ (**4**), which controls the amount of free borane that can lead to over-reduction to methane. Free borane activates the silane by formation of $[R_3Si\text{-}H\cdots B(C_6F_5)_3]$, which can then transfer the silylium (R_3Si^+) fragment to the oxygen atoms of the Ni formate and Ni acetal intermediates. The ion pair $[(PBP)Ni][HB(C_6F_5)_3]$ (**5**) is the key species that activates CO_2 in the catalytic cycle (and silylformate in a second step) with $[HB(C_6F_5)_3]^-$ as the source of

hydride. Hydride transfer to $[(PBP)Ni\text{-}OCO]^+$ is virtually barrier-less whereas hydride transfer to $[(PBP)Ni\text{-}OCHOSiR_3]^+$ has the second highest energy barrier of the process (25.2 $kcal \cdot mol^{-1}$). Therefore, the (PBP)Ni framework is instrumental in both reduction steps of the catalysis and controls the selectivity of the reaction by sequestering $B(C_6F_5)_3$.

KEYWORDS: CO_2, nickel complexes, boryl ligands, hydrosilylation, mechanisms, DFT calculations

INTRODUCTION

Carbon dioxide (CO_2) is present in the atmosphere and its concentration is increasing as a consequence of the intensive use of fossil fuels. Re-use of this non-toxic, renewable and abundant source of carbon as a C1 building block for the synthesis of liquid fuels and added value chemicals is a goal in chemical synthesis that has attracted considerable attention since the first account of its activation by a metal complex,[1] and increasingly during the last decade.[2,3] However, the kinetic inertness and thermodynamic stability of CO_2 make its activation and reduction a challenge that has been tackled by the use of metal complexes[4-6] and organic systems,[7-9] including Frustrated Lewis Pairs (FLP).[10-17] Selective reduction of CO_2 to methanol,[18-22] and also to formic acid[23-29] and methane[30-33] are of great industrial interest, and many efforts have been made to design homogeneous metal catalysts to this end. Formaldehyde is another product of the partial reduction of CO_2, with a worldwide production of over 20 million tons per year, however its current industrial synthesis is based on the catalytic oxidation of methanol at high temperatures.[34] There are comparatively few examples of catalysts capable of reducing CO_2 to the formaldehyde level selectively.[16,17,35-38] Some representative examples

(Scheme 1) include ruthenium and iron catalysts reported by Bontemps and Sabo-Etienne that yield formaldehyde by the selective reduction of CO_2 with borane,[36,37] the ruthenium-catalyzed reduction of CO_2 to bis(silyl)acetal or methyl silyl ether (controlled by the reaction temperature) described by Oestreich et *al*.[38] and the rhenium and scandium complexes of Berke[17] and Piers,[35] who applied the Frustrated Lewis Pair (FLP) concept to the hydrosilylation of CO_2 with $B(C_6F_5)_3$ as co-catalyst.

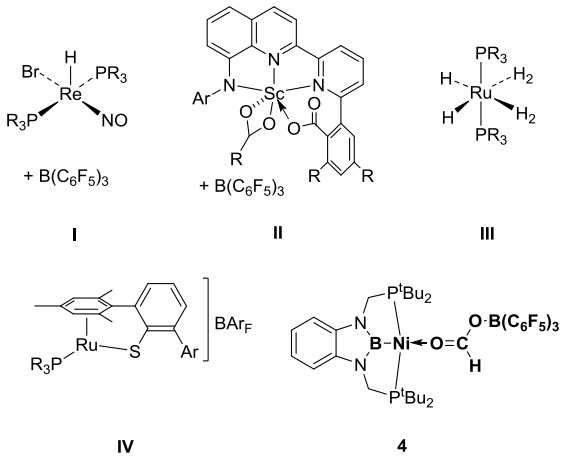

Scheme 1. Examples of catalysts for the selective reduction of CO_2 to the formaldehyde level: **I** Berke, 2013 (reference 17); **II** Piers, 2014 (reference 35); **III** Bontemps and Sabo-Etienne, (reference 37); **IV** Oestreich, 2015 (reference 38) and compound **4** of this work.

Lately we have focused our attention on the reactivity of nickel complexes stabilized by a bis(phosphino)boryl (PBP) ligand.[39-44] Thus, we have reported the synthesis of a nickel methyl complex (PBP)NiMe (**1**), which undergoes hydrogenolysis of its Ni-Me bond with activation of H_2 through a cooperative metal-boryl mechanism to yield the hydride derivative (PBP)NiH (**2**) (Scheme 2).[45]

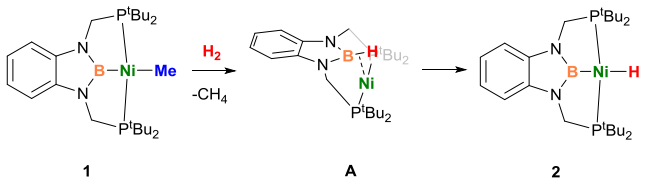

Scheme 2. Formation of 2 via a Ni(0) σ-borane (**A**).

We expected that the strong *trans* influence of the boryl ligand[46-49] would increase the nucleophilicity of the hydride,[50-52] which would in turn make **2** a good candidate to serve as catalyst for the activation of CO_2, since insertion of this molecule into a metal-hydrogen bond is often postulated as a key step in the catalytic conversion of CO_2 by transition metal complexes.[53,54] Indeed, we have recently reported that **2** reacts with CO_2 (1 bar, r.t.) to form the formate complex (PBP)Ni-OCHO (**3**) instantaneously (Scheme 3).[55] The same species **2** and **3** have been synthesized in the group of J. Peters and **3** has been used as olefin hydrogenation catalyst.[49]

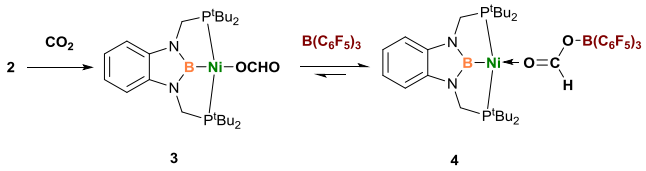

Scheme 3. Synthesis of the catalyst (**4**).

In our case, we have reported that **3** is the precursor of an efficient catalyst for a highly selective hydrosilylation of CO_2 into bis(silyl)acetal with $B(C_6F_5)_3$ as co-catalyst (Scheme 4).[55] The catalyst, (PBP)Ni-OCHO·$B(C_6F_5)_3$ (**4**), was isolated after treatment of **3** with $B(C_6F_5)_3$ and fully characterized by spectroscopic methods including X-Ray diffraction. Catalyst loadings of 0.05% afford high conversions at 70º with various silanes, with turnover numbers up to 1200 and

turnover frequencies up to 56 h^{-1}, which makes **4** one the most active catalysts to date for this transformation.[35]

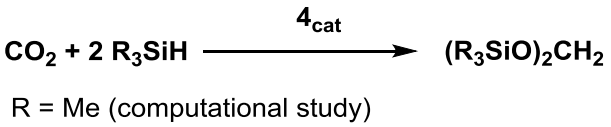

Scheme 4. Reaction catalyzed by **4**. Me_3SiH was used as a model in the computational study.

In this work we report a detailed investigation of the mechanism of such catalysis, which involves a role for the $B(C_6F_5)_3$ co-catalyst in activating the silane and the participation of the (PBP)Ni metal framework in the activation of CO_2 and in controlling the selectivity of the process. We will also briefly probe the effect of the boryl functionality in the insertion of CO_2 into the Ni-H bond of **2** by comparing this molecule with related pincer nickel complexes.

COMPUTATIONAL DETAILS

Density Functional Theory (DFT) calculations[56,57] were carried out using the Gaussian09 (G09) software.[58] All geometries were optimized without restrictions in the gas phase with the PBE0 functional as implemented in the G09 software.[59] Non-metal atoms were described with the 6-31G(d,p) basis set with polarization functions and the nickel atom was modelled with the Stuttgart/Dresden SDD basis set and its associated Electron Core Potential.[60] Vibrational analysis at the same level of theory was carried out to characterize the optimized geometries as minima or saddle points (Transition States, TS) of the Potential Energy Hypersurface as well as for obtaining the corresponding Zero-Point corrections and thermal corrections to Enthalpy and Free Energy. The nature of the species connected by a given TS was established by means of Intrinsic Reaction Coordinate (IRC)[61] calculations or by allowing the TS geometries to vibrate along their imaginary frequency and optimizing the resulting geometries to the nearest minima.

Bulk solvent effects were modelled by single point calculations on the gas phase geometries using Truhlar's SMD continuum solvent model.[62] Empirical dispersion corrections were shown to have substantial effects on the energy barriers of our systems and have also been introduced with the D3 version of Grimme's dispersion[63-65] by single point calculations on the gas phase geometries (optimizing the molecular geometries with the PBE0-D corrected functional yielded very similar results). Exploratory calculations were carried out using a simplified version of the catalyst in which the ^{t}Bu groups on the phosphorus atoms of the PBP ligand were replaced by Me groups (PBP_{Me}, the corresponding species are denoted by a Me subscript). These calculations were used to favor one mechanistic pathway, which was then recalculated with the real catalyst. Also, we have used Me_3SiH instead of larger silanes, however the use of the real Lewis acid, $B(C_6F_5)_3$, in the calculations (instead of BF_3) was shown to be critical to account for the experimental results.

Free energy in solution. Translation entropy, while accurately calculated in the gas phase,[66] is greatly overestimated by standard calculation methods for reactions in solution.[67] Theoretical[67-69] and experimental[70,71] investigations suggest that a 50% correction[72,73] to gas phase entropy (3-6 kcal per mole change) yields better agreement between experimental (solution) and calculated (gas phase) data. Some authors choose to omit entropy data entirely and only use enthalpy values.[74] Throughout the following discussion we will use Zero-Point Energies (with solvent and dispersion corrections) and will indicate 50% corrected-free energy variations (ΔG_{50}) when appropriate.

RESULTS AND DISCUSSION

We have directed our investigations to understanding the role of the (PBP)Ni framework in the reduction of CO_2 and in the selectivity of the catalysis. We begin this section by accounting

for the role of the boryl functionality of **2** in facilitating the insertion of CO_2 into its Ni(II)-H bond. The results described below reflect the prompt formation of precursor **3**. However, it soon became obvious from further experiments that the active species in catalyst is **4**, with $B(C_6F_5)_5$ being instrumental for the reaction to occur. Therefore, we focused subsequent efforts in analyzing the reactivity of **4** with Me_3SiH, with results that are discussed later.

CO_2 insertion into the Ni-H bond of 2. Effect of the boryl functionality. Studies on the insertion of CO_2 into Ni-H and Ni-L (L ≠ H) bonds of related species have been reported and a relationship has been established between the influence of the ligand *trans* to H and the energy barriers of the reactions.[54,52] Insertion of CO_2 into Ni-H bonds does not feature in the catalytic cycle that we describe here, as we shall see below. However, we describe here our study the reaction of **2** with CO_2 by DFT methods as a probe of the *trans*-influence of its boryl moiety. Also, for comparison purposes, we calculated the insertion of CO_2 into Ni(II)-H bonds of analogous pincer complexes with different ligands *trans* to H (Scheme 5). Thus, we used model complexes (with methyl groups on P and N atoms replacing larger substituents) derived from our (PBP_{Me})NiH (**2_{Me}**) and other nickel hydrides containing PCP (**$2_{PCP,Me}$**),[75] POCOP (**$2_{POCOP,Me}$**)[19,76] and PSiP (**$2_{PSiP,Me}$**)[77] ligands. Cationic derivatives containing carbene ($2_{PCBImP,Me}$) and pyridine (**$2_{PNP,Me}$** and **$2_{NNN,Me}$**) ligands *trans* to H were considered in addition.

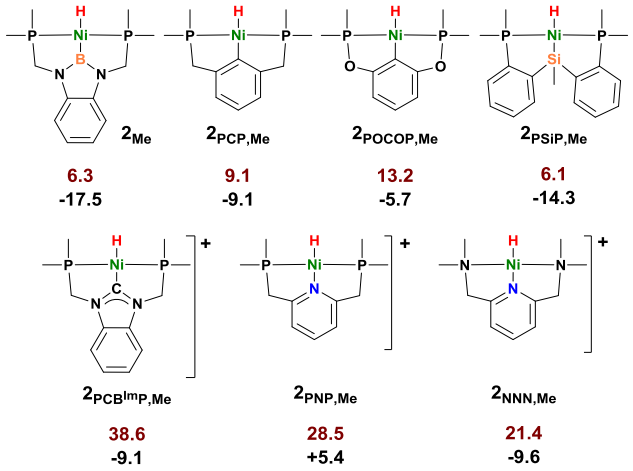

Scheme 5. Energies involved in the insertion of CO_2 into the Ni-H of several pincer complexes: $\Delta G^{\neq}$ (red, top) and ΔG^{0} (bottom). In the cases in which a two-step process is involved (with $\mathbf{2_{PCP,Me}}$ and $\mathbf{2_{PSiP,Me}}$) the highest barrier from the reactants is reported.

All insertion reactions are thermodynamically favorable except for the PNP species. Analysis of the insertion mechanism of the reaction with $\mathbf{2_{Me}}$ (Figure 1) reveals that nucleophilic attack of the hydride ligand to CO_2 takes place at the transition state, without involvement of the nickel atom, whereas, in agreement with previous analysis,[54] the remaining systems feature four-centered transition states with participation of the metal (see the SI for details). Additionally, two-step mechanisms were found for the PSiP and PCP systems at our level of theory, in which formation of the formate ligand is preceded by the generation of an activated [Ni]-H·CO_2 complex with very short H···CO_2 contacts. As expected, the PSiP and $\mathbf{2_{Me}}$ complexes yielded the lowest overall barriers for CO_2 insertion, $\Delta G^{\neq}$ = 6.1 and 6.3 kcal·mol^{-1} respectively, in good agreement with the strong *trans* influence of silyl and boryl ligands.[46-49] Additionally, $\mathbf{2}_{Me}$ yields the most stable Ni formate complex of all the species calculated. Cationic species presented higher insertion barriers, with insertion of CO_2 in $2_{\mathbf{PCBImP,Me}}$, resulting from the formal

replacement of the boron of $\mathbf{2_{Me}}$ by a carbon atom, being the most endoergic. Moreover, the trends obtained in this study are consistent with the experimental observations in terms of the time required for the reaction to complete at room temperature; while $\mathbf{2_{Me}}$ (energy barrier of 6.3 kcal·mol^{-1}) gives the formate **3** in a few seconds,[55] the PCP ($\mathbf{2_{PCP,Me}}$; $\Delta G^{\neq}$ = 9.1 kcal·mol^{-1}) and POCOP complexes ($\mathbf{2_{POCOP,Me}}$; $\Delta G^{\neq}$ = 13.2 kcal·mol^{-1}) require a few minutes[75] and one hour[76] respectively.

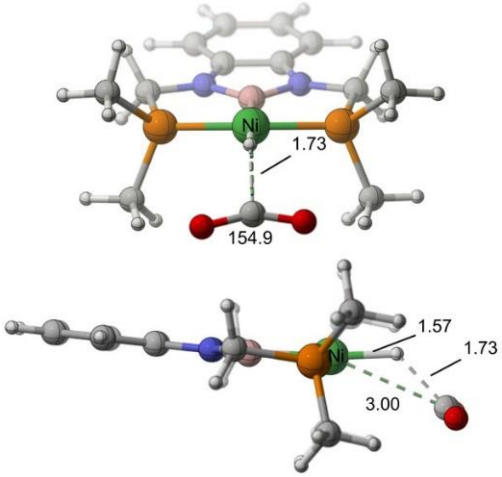

Figure 1. Front and side views of the transition state for insertion of CO_2 into the Ni-H bond of $\mathbf{2_{Me}}$.

Catalysis by 4. Role of $B(C_6F_5)_3$. The nature of **4**, (PBP)Ni-OCHO·$B(C_6F_5)_3$, as the catalyst was established experimentally.[55] Three experimental facts have been taken into consideration to propose mechanistic pathways for the reaction (Scheme 6):

1. Addition of one equivalent of Et_3SiH to a 1:1 mixture of **3** and $B(C_6F_5)_3$ (**4** forms *in situ*) results in the complete consumption of the silane and formation of the bis(silyl)acetal derivative after heating at 70 ºC for 30 min. No silylformate was detected at any stage of this transformation.

2. ^{1}H NMR-monitoring of the CO_2 reduction in catalytic conditions, using ^{13}C-enriched CO_2, showed $(Et_3SiO)_2CH_2$ as the almost exclusive reduction product.[78] Intentional addition of $B(C_6F_5)_3$ following consumption of CO_2 (after 8h) resulted in the quantitative reduction of $(Et_3SiO)_2CH_2$ to methane.
3. When an NMR sample of **4** synthesized using $^{13}CO_2$ was charged with non-labelled CO_2 (1 bar), 12% CO_2 exchange was observed after 22 h at 70 ºC.

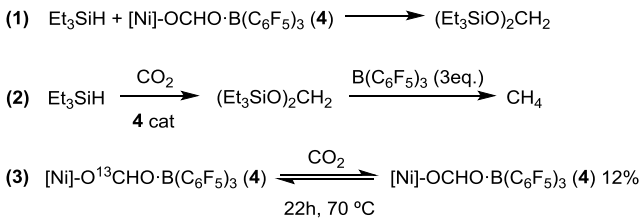

Scheme 6. Relevant experimental observations.

The DFT-optimized geometry of **4** is in agreement with the solid state (X-Ray) data (Figure S4).[55] Elongation of the Ni-O bond from 1.958 in **3** to 1.997 Å upon $B(C_6F_5)_3$ coordination is also in agreement with experimental data by Peters[49] and us,[55] and the linkage of the formaborate group is in agreement with the zwitterionic structure depicted in Scheme 3[31,35,79] with NiO=C and C-OB distances of 1.239 and 1.277 Å respectively. The B-O distance, 1.558 Å, is similar to related species formed by CO_2 insertion into Frustrated Lewis Pairs adducts.[80,81]

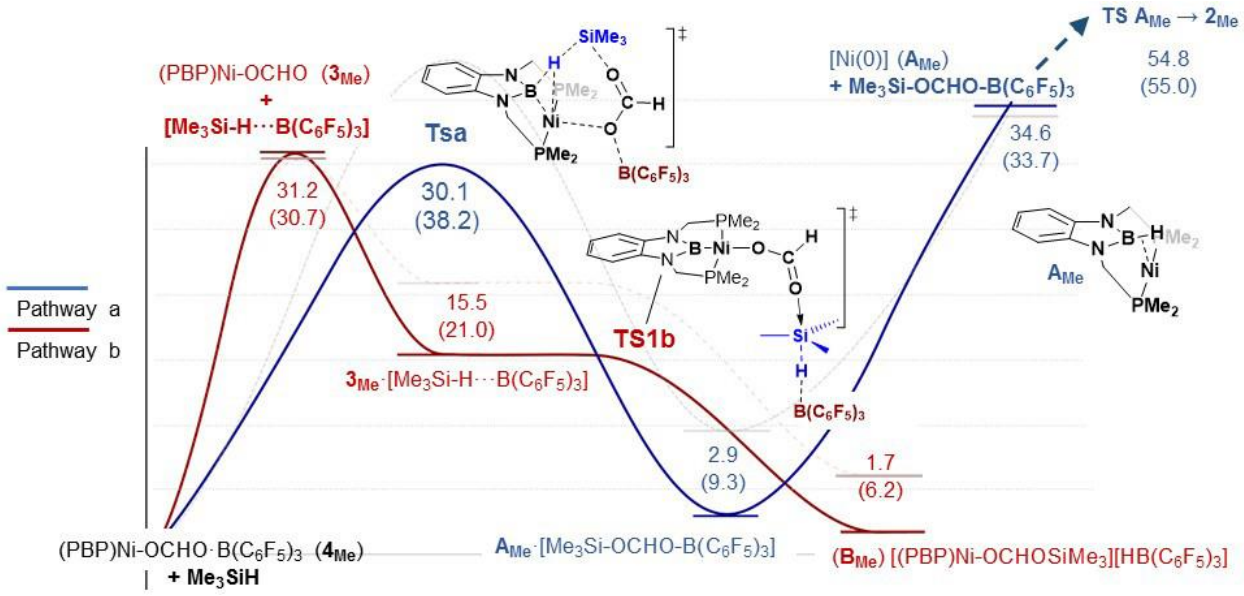

Figure 2. (double column) Initial steps of the pathways considered for the reduction of CO_2 to the formate level by $\mathbf{4_{Me}}$ and Me_3SiH (model system). Pathway a) (blue trace) involves direct hydrosilylation of the catalyst whereas pathway b) (red trace) requires $B(C_6F_5)_3$ dissociation. The profiles represent ΔZPE in kcal·mol^{-1} (ΔG_{50} data in parentheses).

I. Reduction to the formate level. We have considered two possible pathways for the catalysis by **4**. These begin with either: a) *direct* hydrosilylation of the catalyst[82] or b) silane activation by the borane previously dissociated from the catalyst (Figure 2). The model system ($\mathbf{4_{Me}}$ + Me_3SiH) was used in these exploratory calculations.

Silane attack to $\mathbf{4_{Me}}$ (a) was considered to take place from the side of the coordination plane of Ni further away from the $B(C_6F_5)_3$ fragment, with the Si atom approaching the Ni-coordinated oxygen. At the transition state (Figures 2 and S5), slippage of the formaborate ligand has taken place with splitting of the former Ni-O bond and formation of a new Ni-O interaction with the boron-bonded oxygen ($d_{Ni\cdots O}$ = 2.25 Å). Simultaneously, a new Si-O bond begins to form ($d_{Si\cdots O}$ = 2.02 Å) as hydrogen transfer takes place from Si-H to the boryl fragment ($d_{B\cdots H}$ = 1.67 Å).

The Ni atom does not form a Ni-H bond,[83] instead the transition state leads to a Ni(0) species featuring a σ-borane interaction,[41] which forms an adduct with $Me_3SiOCHOB(C_6F_5)_3$ ($\mathbf{A_{Me}}$·$Me_3SiOCHOB(C_6F_5)_3$). This situation is reminiscent of the mechanism that we described for the hydrogenolysis of **1**,[45] in which H_2 was activated at the nickel center, with cooperation of the boryl moiety. The barrier for Si-H activation from $\mathbf{4}_{Me}$ + Me_3SiH is $\Delta ZPE^{\neq}$ = 30.1 kcal·mol^{-1} ($\Delta G_{50}^{\neq}$ = 38.2 kcal·mol^{-1}).

Pathway b) requires dissociation of $B(C_6F_5)_3$ from $\mathbf{4}_{Me}$ to activate the silane by formation of $[Me_3Si\text{-}H\cdots B(C_6F_5)_3]$.[80,84-86] The energy variation in this case is 31.2 kcal·mol^{-1} (ΔG_{50} = 30.7 kcal·mol^{-1}). This species increases the electrophilicity of Si, making it more prone to nucleophilic attack by the carbonyl of (PBP_{Me})Ni-OCHO ($\mathbf{3_{Me}}$).[87] This process (**TS1b**) can be related to a Frustrated Lewis Pair (FLP) bond activation as described by Piers and Tuonomen,[85] in which the Ni formate complex and the borane are the Lewis base and Lewis acid respectively (Scheme 7).

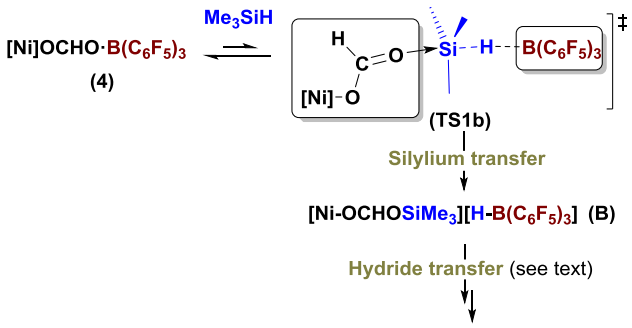

Scheme 7. Frustrated Lewis Pair-Like Si-H activation allows transfer of silylium (R_3Si^+) to the formate ligand of the catalyst.

While both pathways require overcome comparable initial energy barriers, in pathway a) separation of the $\mathbf{A_{Me}}$ and $Me_3SiOCHOB(C_6F_5)_3$ fragments is endothermic by a further 31.7 kcal·mol^{-1} and, when regeneration of $\mathbf{2_{Me}}$ from $\mathbf{A_{Me}}$ (to insert more CO_2) is taken into account, the overall energy barrier from the reactants amounts to 54.8 kcal·mol^{-1}. On the contrary, borane dissociation is the highest energy barrier of pathway b). Thus, FLP-like bond activation of silane at the encounter complex $\mathbf{3_{Me}}$·[Me_3Si-H···$B(C_6F_5)_3$], which lays 15.5 kcal·mol^{-1} above the origin, occurs with S_N2-like transfer of silylium to (PBP_{Me})Ni-OCHO[84] (Scheme 7 and Figure 2) with virtually no energy barrier ($\Delta E^{\neq}$(**TS1b**) < 1 kcal·mol^{-1}). At the transition state B···H, H···Si and Si···O distances are 1.38, 1.65 and 2.81 Å respectively. The resulting ion pair [(PBP_{Me})Ni-$OCHOSiMe_3$][$HB(C_6F_5)_3$] ($\mathbf{B_{Me}}$) lays 1.7 kcal·mol^{-1} above $\mathbf{4_{Me}}$ + Me_3SiH (Figure S6). These results indicated that pathway a) should be discarded and from this point we will describe the results obtained with the real catalyst for pathway b).

Results with the full catalyst 4. Dissociation of $B(C_6F_5)_3$ from **4** to yield (PBP)Ni-OCHO (**3**) + [Me_3Si-H···$B(C_6F_5)_3$] has a calculated energy variation of ca. 30 kcal·mol^{-1} (Figure 3). As in the model system, this is the most endothermic (and endergonic) step of this pathway. Me_3Si^+ transfer from [Me_3Si-H···$B(C_6F_5)_3$] to the O-terminus of **3** yields the ion pair **B**, [(PBP)NiOCHO$SiMe_3$][$HB(C_6F_5)_3$], with an energy return of 27.5 kcal·mol^{-1} from **3** + [Me_3Si-H···$B(C_6F_5)_3$]. All attempts to locate the corresponding transition state (**TS1b**) resulted either in separation of **3** and [Me_3Si-H···$B(C_6F_5)_3$] or in evolution of the guessing geometries to **B**. This, in addition to the results of a Relaxed Potential Energy Scan (PES; Figure S7) and the low energy barrier calculated for the model system supports that silylium transfer at this step is very facile. Rearrangement of the relative positions of the cation and anion of **B** affords a geometry for the ion pair, **B'** (Figure S8), that is more stable than the former by 11.6 kcal·mol^{-1}, and from

which the $[HB(C_6F_5)_3]^-$ anion can either a) approach the Ni atom with extrusion of $Me_3SiOCHO$ to generate [(PBP)Ni][$HB(C_6F_5)_3$] (**5**) (Figure S9), or b) transfer H^- to the formate ligand (**C**) to initiate the second reduction step (Scheme 8). The former step (a) has an energy cost of 25.2 kcal·mol^{-1} ($\Delta G_{50}^{\neq}$ = 19.7 kcal·mol^{-1}) from **B'**, which is similar, as we shall see, to the energy required for H^- transfer (b). However, experiments showing the formation of bis(silyl)acetal, $(Et_3SiO)_2CH_2$, as the sole product of the reduction of CO_2 by a 1:1 mixture of **4** and Et_3SiH[55] (Scheme 6) strongly indicate that the second reduction process must be faster than extrusion of silylformate followed by regeneration of **4** from **5**.

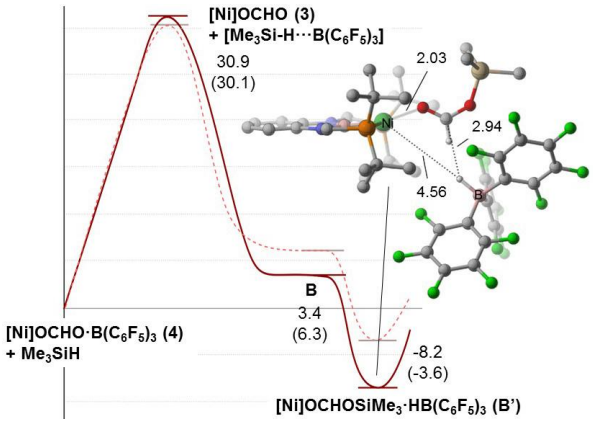

Figure 3. Energy profile of the first reduction stage calculated with the real catalyst. Δ*ZPE* data in kcal·mol^{-1} (ΔG_{50} data in parentheses and dashed trace). The inset represents the optimized geometry of ion pair **B'** (most C-*H* atoms omitted for clarity).

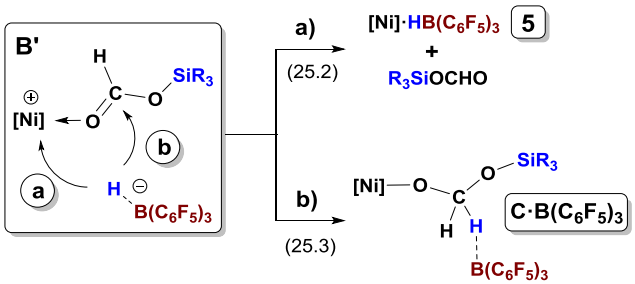

Scheme 8. Evolution of intermediate **B'** (overall Zero-Point Energies, in kcal·mol^{-1}, from **B'** in parentheses).

II. Second reduction stage. Hydride transfer from the hydroborate $[HB(C_6F_5)_3]^-$ to the formate ligand of **B'** yields (PBP)Ni-OCH_2OSiMe_3·BAr_3, **C**·$B(C_6F_5)_3$, which lays 25.3 kcal·mol^{-1} (ΔG_{50}^0 = 24.6 kcal·mol^{-1}) above **B'** (Scheme 8 and Figure 4). Unfortunately, no TS has been located for the transfer, however, like in the first silylium transfer step (**TS1b**), calculations on the model system rendered the reverse process (**TS2b**; $\mathbf{C}_{Me}$·$B(C_6F_5)_3$ →$\mathbf{B'}_{Me}$) virtually barrier-less, which was again supported by a relaxed PES on the real system (Figure S10). The borane is loosely bound to the organometallic fragment of **C**·$B(C_6F_5)_3$ and can activate a new molecule of silane to form the new encounter complex **C**·[Me_3Si-H···$B(C_6F_5)_3$] (Figure S11) (ΔZPE^0 = 11.7 kcal·mol^{-1} from the origin), from which a second Me_3Si^+ fragment is transferred, S_N2 fashion, in this case to the Ni-bound oxygen of the acetal ligand (**TS3b**). Again this step is very fast (when solvent and dispersion corrections are applied $\Delta ZPE^{\neq}$ and $\Delta G_{50}^{\neq}$ from **C**·[Me_3Si-H···$B(C_6F_5)_3$] are nearly zero) and the formation of the new ion pair [(PBP)Ni-$O(SiMe_3)CH_2OSiMe_3$][$HB(C_6F_5)_3$)] (**D**) is exothermic by 22.7 kcal·mol^{-1}. Interestingly, if dispersion and entropy corrections are not applied, $\Delta G^{\neq}$ for this step exceeds 50 kcal·mol^{-1} from the origin, whereas if only dispersion corrections are included $\Delta G^{\neq}$ = 36.9 kcal·mol^{-1}. The former value of free energy would imply that the reaction cannot take place via any of the two mechanisms considered, and the latter, even if it could be justified, predicts the second reduction stage being slower than the first one (*i.e.* $Me_3SiOCHO$ would be the main product), contrary to the experimental observations. These results highlight the importance of both dispersion

corrections in large systems and also the need for entropy corrections for reactions in solution. In this case, the entropy penalty is larger during the second reduction stage, since the variation in the number of species from the reactants to the products is up to -2, whereas in the first reduction stage is up to -1. Finally, extrusion of $(Me_3SiO)_2CH_2$ from **D** yields **5** and is exothermic by 23.1 kcal·mol^{-1} from **C**·[Me_3Si-H···$B(C_6F_5)_3$] ($\Delta G_{50}{}^0$ = -29.2 kcal·mol^{-1}). The overall reaction, when regeneration of the catalyst, **4**, from **5** is considered (see below) is exothermic by 46.3 kcal·mol^{-1} ($\Delta G_{50}{}^0$ = -39.0 kcal·mol^{-1}). The overall energy profile, including the regeneration of the catalyst can be found in the supporting information.

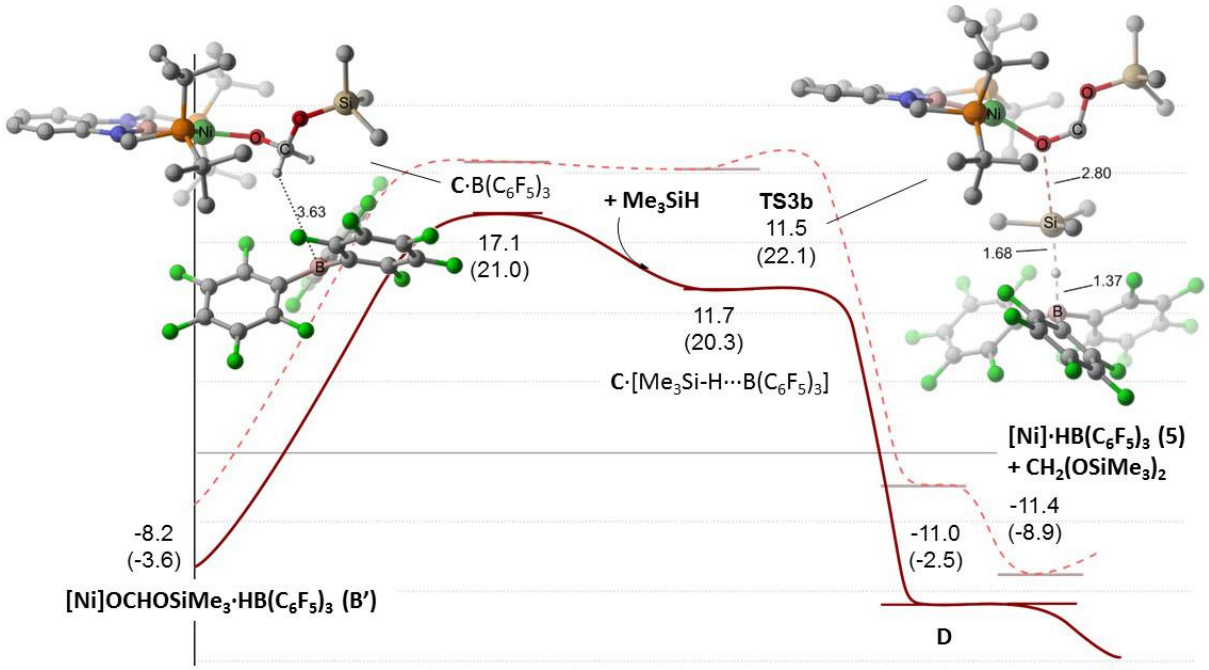

Figure 4 (please, double column). Energy profile for the second reduction stage. Δ*ZPE* in kcal·mol^{-1} from **4** + Me_3SiH –solid trace- (ΔG_{50} data in parentheses and dashed trace).

III. Regeneration of the catalyst. CO_2 activation by [(PBP)Ni][$HB(C_6F_5)_3$] (5). The reaction media remains homogeneous for as long as CO_2 is present. Once it is consumed a precipitate appears, which readily re-dissolves when more CO_2 is added, thus regenerating **4**. We

attribute such precipitate to the Ni hydridoborate complex **5**, [(PBP)Ni][HB(C_6F_5)$_3$]. Evidence of the formation of **5** has been obtained by NMR spectroscopy. ^{1}H{^{11}B} NMR of the precipitate in toluene-d_8 shows the expected signals for the (PBP)Ni core and a broad resonance centered δ 4.38 ppm attributable to the B*H*. Correspondingly, ^{11}B NMR experiments reveal the characteristic resonance of the boryl boron from the PBP as a singlet at 28.3 in addition to a doublet resonance for the *B*H at δ -24.4 ppm with $^1J_{BH}$ = 93 Hz, which simplifies upon ^{1}H decoupling.[33,88,89] Unfortunately, small amounts of THF or other ethereal solvents had to be added to the samples of **5** in order to achieve sufficient solubility, therefore amounts of ether-borane adducts are seen by NMR[90] (see the SI for further details).

We have already shown how **5** must be formed after extrusion of bis(silyl)acetal from **D**, and could also be formed after the first reduction process from **4** (Scheme 8a). According to our calculations, activation of CO_2 by **5** may follow a mechanism which is comparable to that proposed by Piers, Maron and Eisenstein for the analogous reaction with the ion pair [Cp*$_2$Sc][HB(C_6F_5)$_3$].[31] Indeed, **5** is best described as a contact ion pair, in which the hydridoborate may bind the nickel in either κ^1-*F* or κ^1-*H* manners. DFT calculations located two minima for **5** within 1.4 kcal·mol^{-1}, featuring κ^1-*F* and κ^1-*H* interactions between the metal and hydridoborate fragments (Figure 5).

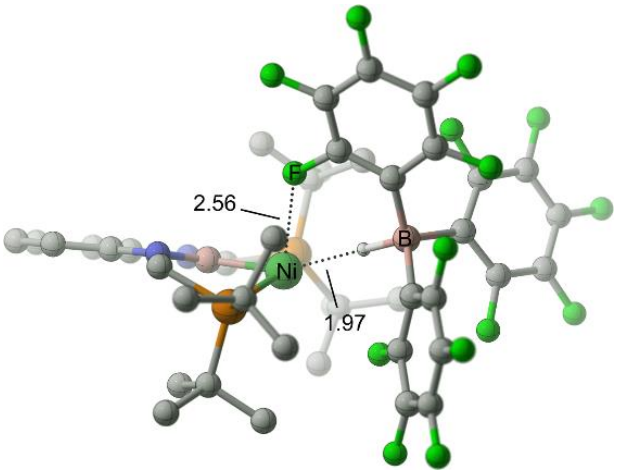

Figure 5. Molecular geometry of [(PBP)Ni][$HB(C_6F_5)_3$] (**5**). H atoms have been omitted for clarity.

Insertion of CO_2 in the pocket between these fragments is exothermic by 4.6 kcal·mol^{-1} (from κ^1-*F* coordinated **5** + CO_2; $\Delta G_{50}{}^0$= 0.0 kcal·mol^{-1}), and yields **E**, [(PBP)Ni-OCO][$HB(C_6F_5)_3$] (Figure 6) featuring κ^1-*O* CO_2 coordination to the metal.[91] An early transition state (**TS4**) was located for H^- transfer from the borohydride to coordinated CO_2, 0.4 kcal·mol^{-1} above the previous minimum. At this TS, the B-H bond is very slightly elongated by 0.03 Å, the O-C-O angle is 160º and the C···H distance is still long at 1.77 Å. In the product of this step (**F**), which lays 6.1 kcal·mol^{-1} below **5 + CO_2**, the new HCO_2^- ligand interacts with $B(C_6F_5)$ through a H···B contact of 2.36 Å. Borane coordination to the O-termini of the formate is very exothermic and requires overcoming a barrier of only 2.3 kcal·mol^{-1}. The overall process is nearly barrier-less and has an energy return of ca. 35 kcal·mol^{-1} ($\Delta G_{50}{}^0$= 30.4 kcal·mol^{-1}), in agreement with the observed instantaneous re-dissolution of **5** to regenerate **4** upon CO_2 addition to the reaction mixture, and with the CO_2 exchange equilibrium (3) of Scheme 6, as the limited incorporation of $^{13}CO_2$ in **4** indicates that the reverse reaction of CO_2 dissociation presents a high barrier.

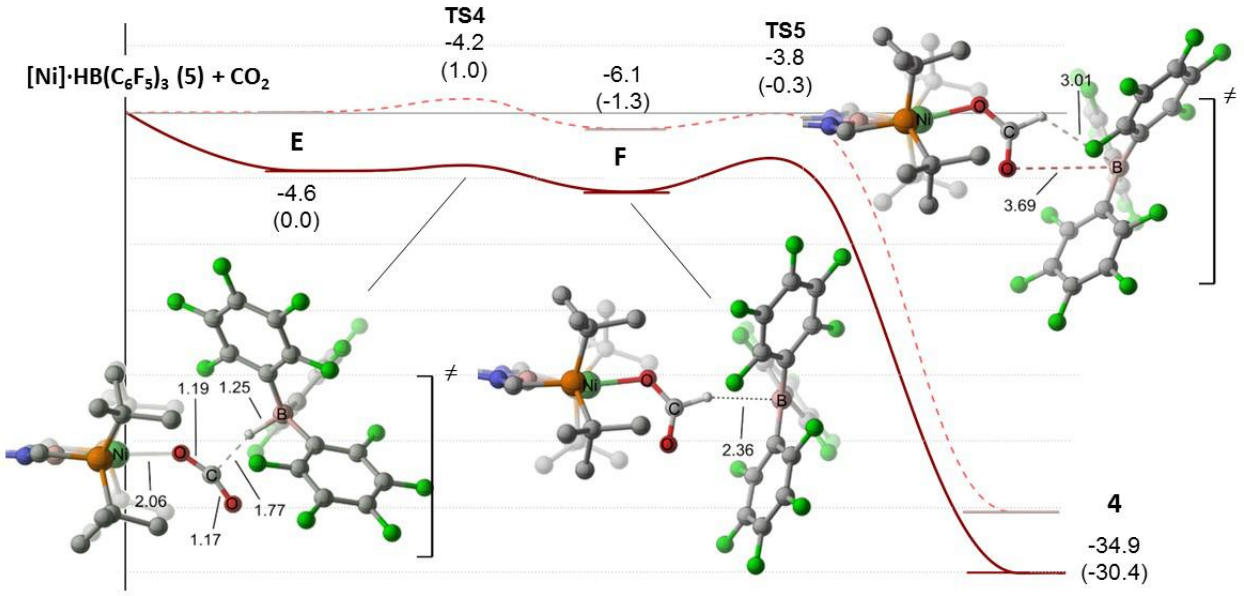

Figure 6 (please, double column). Energy profile for CO_2 activation by the ion pair [(PBP)Ni][$HB(C_6F_5)_3$] (**5**) to regenerate the catalyst **4**. ΔZPE in kcal·mol^{-1} –solid line- (ΔG_{50} in parentheses –dashed line-).

The overall catalytic cycle is represented in Scheme 9: borane dissociation from the catalyst allows the formation of small amounts of [Me_3Si-H···$B(C_6F_5)_3$], which readily transfer silylium to the formate ligand of **3**. Hydride transfer to the silylformate of the intermediate **B** gives **C·B(C_6F_5)$_3$** and must be faster than extrusion of the organic fragment with formation of the ion pair [(PBP)Ni][$HB(C_6F_5)_3$], **5**. Then, a second molecule of silane reacts with **C·B(C_6F_5)$_3$** to yield more [Me_3Si-H···$B(C_6F_5)_3$], which transfers a second silylium to the silylacetal ligand of **C**. Extrusion of the bis(silyl)acetal yields **5**, which is able to activate CO_2 to close the cycle.

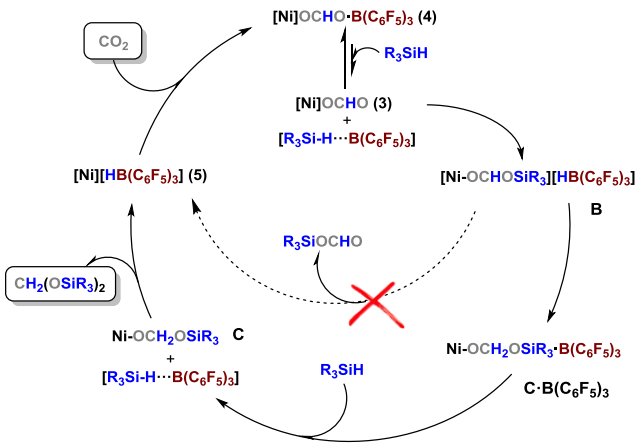

Scheme 9. Overall catalytic cycle.

IV. Origin of the selectivity. Due to its remarkable stability, the first step in CO_2 reduction is often the most difficult. In our case, it seems clear that the (PBP)Ni framework is responsible for this process, either by facile CO_2 insertion into the Ni-H bond of **2** thanks to the *trans* influence that the boryl moiety exerts on this bond, or via CO_2 insertion into the components of the contact ion complex [(PBP)Ni][$HB(C_6F_5)_3$] (**5**) followed by hydride transfer, as we have described before. However, most reactions that reduce CO_2 with silanes and $B(C_6F_5)_3$ co-catalyst yield methane.[30-33,80,92] This is due in most cases to the formation of [$R_3Si\text{-}H\cdots B(C_6F_5)_3$], which is an active catalyst in the reduction of carbonyl groups,[84,85,93] although it is not capable of activating CO_2 on its own.[15] Therefore, sequestration of $B(C_6F_5)_3$ by the metal framework is required for selectivity control. Thus Piers, Maron and Eisenstein reported[31] that a ca. 1:1 $(Et_2SiO)_2CH_2$:CH_4 mixture was formed in the reduction of CO_2 by [Cp*Sc]·[$HB(C_6F_5)_3$] with Et_3SiH in the absence of added borane, and calculated that $B(C_6F_5)_3$ dissociation from [Cp*ScOCOH]·$B(C_6F_5)_3$ is relatively accessible with ΔG^0= 6.4 kcal·mol^{-1}. In a subsequent work Piers et al. argued that increased selectivity towards bis(silyl)acetal was achieved thanks to a more effective trapping of $B(C_6F_5)_3$ by a modified Sc catalyst.[35]

In our case, we have already indicated that borane dissociation from **4** (Scheme 10, eq. 1) is highly disfavored. The same is true for borane dissociation from **5** to give **2** (Scheme 10, eq 2). $\Delta G_{50}{}^{0}$ for these processes are 27.9 and 24.2 kcal·mol^{-1} respectively. In addition, activation of CO_2 and $Me_3SiOCHO$ compete favorably with the latter process. Dissociation of borane could also occur from (PBP)Ni-OCH_2OSiMe_3·$B(C_6F_5)_3$ (**C**·$B(C_6F_5)_3$), but the process from (**4**) + $2Me_3SiH$ is again endoergic, with $\Delta G_{50}{}^{0}$= 22.3 kcal·mol^{-1}. When this process is combined with the formation of $Me_3SiOCHO$ from (**4**) + Me_3SiH (Scheme 10, eq. 3) the overall free energy involved amounts to $\Delta G_{50}{}^{0}$= 38.4 kcal·mol^{-1}. Formation of $(Me_3SiO)_2CH_2$ via reduction of $Me_3SiOCHO$ with [Et_3Si-H···$B(C_6F_5)_3$)] is not exoergic enough ($\Delta G_{50}{}^{0}$= -17.7 kcal·mol^{-1}) to make the overall process thermodynamically favorable. These data support that in our case both CO_2 reduction processes are metal mediated, and explain how over reduction is controlled by our catalyst.

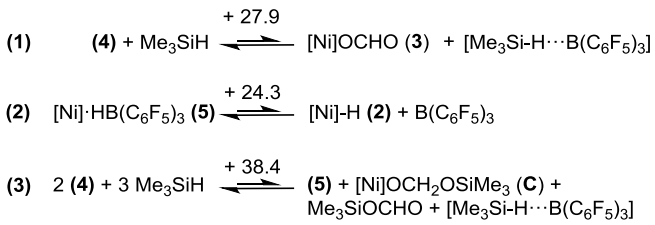

Scheme 10. Relevant equilibria related to $B(C_6F_5)_3$ release and ΔG_{50} (kcal·mol^{-1}) for the forward reaction.

CONCLUDING REMARKS

We have described a mechanism for the selective reduction of CO_2 to the formate level with silanes, catalyzed by a (PBP)Ni complex with $B(C_6F_5)_3$ as co-catalyst.[55] From a computational point of view the use of empirical dispersion corrections has proven to be necessary to account

for the experimental results, as well as it is important to correct the translational entropy, which is overestimated in reactions taking place in solution. The role of the boryl ligand in lowering the energy barrier for stoichiometric insertion of CO_2 into the Ni-H bond of the catalyst precursor **2** has been shown. More importantly, the metal framework has been revealed to be instrumental in the reduction steps during catalysis via FLP-like bond activation steps involving silylium transfer from $[R_3Si\text{-}H\cdots B(C_6F_5)_3]$, followed by hydride transfer from $[HB(C_6F_5)_3]^-$ at contact ion pairs like $[(PBP)Ni][HB(C_6F_5)_3]$[31], which is the species responsible for CO_2 activation. The metal framework is also involved in determining the selectivity of the catalysis, since it does effectively sequester $B(C_6F_5)_3$, thus limiting the amount of $[R_3Si\text{-}H\cdots B(C_6F_5)_3]$ in the reaction medium, and preventing that the latter species catalyzes the reduction of carbonyl groups to CH_4. Therefore, the metal complex takes part in both reduction steps, from CO_2 to $R_3SiOCHO$ and from there to $(R_3SiO)_2CH_2$. We are currently expanding the scope of the (PBP)Ni framework as a catalyst in small molecule activation reactions.

AUTHOR INFORMATION

Corresponding Authors

*joaquin.lopez@iiq.csic.es, *marodriguez@iiq.csic.es

Author Contributions

The manuscript was written through contributions of all authors.

ASSOCIATED CONTENT

Supporting Information. XYZ coordinates and potential energy of calculated species. Additional computational and experimental details. This material is available free of charge via the Internet at http://pubs.acs.org.

ACKNOWLEDGMENT

Financial support (FEDER contribution) from the MINECO (Projects CTQ2013-45011-P and CTQ2014-51912-REDC) and the Junta de Andalucía (Project FQM-2126) is gratefully acknowledged. The use of computational facilities of The Supercomputing Center of Galicia (CESGA) are thankfully acknowledged. J.L.-S. also thanks Dr. Marta Roselló-Merino and Dr. Jesús Campos for useful discussion.

REFERENCES

(1) Aresta, M.; Nobile, C. F.; Albano, V. G.; Forni, E.; Manassero, M. *J. Chem. Soc., Chem. Comm*. **1975**, 636-637.

(2) Liu, Q.; Wu, L.; Jackstell, R.; Beller, M. *Nat. Commun*. **2015**, *6*, 5933.

(3) Wu, L.; Liu, Q.; Jackstell, R.; Beller, M. *Top. Organomet. Chem*. **2016**, *53*, 279-304.

(4) Leitner, W. *Coord. Chem. Rev*. **1996**, *153*, 257-284.

(5) Walther, D.; Ruben, M.; Rau, S. *Coord. Chem. Rev.* **1999**, *182*, 67-100.

(6) Fernandez-Alvarez, F. J.; Aitani, A. M.; Oro, L. A. *Catal. Sci. Technol*. **2014**, *4*, 611-624.

(7) Fiorani, G.; Guo, W.; Kleij, A. W. *Green Chem.* **2015**, *17*, 1375-1389.

(8) Murphy, L. J.; Robertson, K. N.; Kemp, R. A.; Tuononen, H. M.; Clyburne, J. A. C. *ChemCommun* **2015**, *51*, 3942-3956.

(9) Villiers, C.; Dognon, J.-P.; Pollet, R.; Thuéry, P.; Ephritikhine, M. *Angew. Chem. Int. Ed*. **2010**, *49*, 3465-3468.

(10) Stephan, D. W. *Acc. Chem. Res*. **2015**, *48*, 306-316.

(11) Stephan, D. W. *J. Am. Chem. Soc*. **2015**, *137*, 10018-10032.

(12) Stephan, D. W.; Erker, G. *Angew. Chem. Int. Ed.* **2015**, *54*, 6400-6441.

(13) Mömming, C. M.; Otten, E.; Kehr, G.; Fröhlich, R.; Grimme, S.; Stephan, D. W.; Erker, G. *Angew. Chem. Int. Ed*. **2009**, *48*, 6643-6646.

(14) Das Neves Gomes, C.; Blondiaux, E.; Thuéry, P.; Cantat, T. *Chem. Eur. J*. **2014**, *20*, 7098-7106.

(15) von Wolff, N.; Lefèvre, G.; Berthet, J.-C.; Thuery, P.; Cantat, T. *ACS Catal*. **2016**, *6*, 4526-4535.

(16) Declercq, R.; Bouhadir, G.; Bourissou, D.; Légaré, M.-A.; Courtemanche, M.-A.; Nahi, K. S.; Bouchard, N.; Fontaine, F.-G.; Maron, L. *ACS Catal*. **2015**, *5*, 2513-2520.

(17) Jiang, Y.; Blacque, O.; Fox, T.; Berke, H. *J. Am. Chem. Soc.* **2013**, *135*, 7751-7760.

(18) Li, Y.-N.; Ma, R.; He, L.-N.; Diao, Z.-F. *Cat. Sci. Technol.* **2014**, *4*, 1498-1512.

(19) Chakraborty, S.; Zhang, J.; Krause, J. A.; Guan, H. *J. Am. Chem. Soc*. **2010**, *132*, 8872-8873.

(20) Tominaga, K.-i.; Sasaki, Y.; Watanabe, T.; Saito, M. Bull. Chem. Soc. Jpn. **1995**, *68*, 2837-2842.

(21) Huff, C. A.; Sanford, M. S. *J. Am. Chem. Soc*. **2011**, *133*, 18122-18125.

(22) Wesselbaum, S.; Moha, V.; Meuresch, M.; Brosinski, S.; Thenert, K. M.; Kothe, J.; Stein, T. v.; Englert, U.; Holscher, M.; Klankermayer, J.; Leitner, W. *Chem. Sci*. **2015**, *6*, 693-704.

(23) Hull, J. F.; Himeda, Y.; Wang, W.-H.; Hashiguchi, B.; Periana, R.; Szalda, D. J.; Muckerman, J. T.; Fujita, E. *Nat. Chem*. **2012**, *4*, 383-388.

(24) Federsel, C.; Boddien, A.; Jackstell, R.; Jennerjahn, R.; Dyson, P. J.; Scopelliti, R.; Laurenczy, G.; Beller, M. *Angew. Chem. Int. Ed*. **2010**, *49*, 9777-9780.

(25) Kang, P.; Cheng, C.; Chen, Z.; Schauer, C. K.; Meyer, T. J.; Brookhart, M. *J. Am. Chem. Soc*. **2012**, *134*, 5500-5503.

(26) Tanaka, R.; Yamashita, M.; Nozaki, K. *J. Am. Chem. Soc*. **2009**, *131*, 14168-14169.

(27) Lalrempuia, R.; Iglesias, M.; Polo, V.; Sanz Miguel, P. J.; Fernández-Alvarez, F. J.; Pérez-Torrente, J. J.; Oro, L. A. *Angew. Chem. Int. Ed*. **2012**, *51*, 12824-12827.

(28) Jeletic, M. S.; Mock, M. T.; Appel, A. M.; Linehan, J. C. *J. Am. Chem. Soc*. **2013**, *135*, 11533-11536.

(29) Moret, S.; Dyson, P. J.; Laurenczy, G. *Nat. Commun*. **2014**, *5*, 4017.

(30) Matsuo, T.; Kawaguchi, H. *J. Am. Chem. Soc*. **2006**, *128*, 12362-12363.

(31) Berkefeld, A.; Piers, W. E.; Parvez, M.; Castro, L.; Maron, L.; Eisenstein, O. *Chem. Sci*. **2013,** *4*, 2152-2162.

(32) Park, S.; Bézier, D.; Brookhart, M. *J. Am. Chem. Soc*. **2012**, *134*, 11404-11407.

(33) Mitton, S. J.; Turculet, L. *Chem. Eur. J.* **2012**, *18*, 15258-15262.

(34) Reuss, G.; Disteldorf, W.; Gamer, A. O.; Hilt, A. In *Ullmann's Encyclopedia of Industrial Chemistry*, 6th ed.; Willey-VCH: Weinheim, **2002**; Vol 15, p 735.

(35) LeBlanc, F. A.; Piers, W. E.; Parvez, M. *Angew. Chem. Int. Ed*. **2014**, *53*, 789-792.

(36) Jin, G.; Werncke, C. G.; Escudié, Y.; Sabo-Etienne, S.; Bontemps, S. *J. Am. Chem. Soc*. **2015**, *137*, 9563-9566.

(37) Bontemps, S.; Vendier, L.; Sabo-Etienne, S. *J. Am. Chem. Soc*. **2014**, *136*, 4419-4425.

(38) Metsänen, T. T.; Oestreich, M. *Organometallics* **2015**, *34*, 543-546.

(39) Segawa, Y.; Yamashita, M.; Nozaki, K. *J. Am. Chem. Soc*. **2009**, *131*, 9201-9203.

(40) Segawa, Y.; Yamashita, M.; Nozaki, K. *Organometallics* **2009**, *28*, 6234-6242.

(41) Hasegawa, M.; Segawa, Y.; Yamashita, M.; Nozaki, K. *Angew. Chem. Int. Ed*. **2012**, *51*, 6956-6960.

(42) Ogawa, H.; Yamashita, M. *Dalton Trans*. **2013**, *42*, 625-629.

(43) Miyada, T.; Yamashita, M. *Organometallics* **2013**, *32*, 5281-5284.

(44) Hill, A. F.; Lee, S. B.; Park, J.; Shang, R.; Willis, A. C. *Organometallics* **2010**, *29*, 5661-5669.

(45) Curado, N.; Maya, C.; López-Serrano, J.; Rodríguez, A. *ChemCommun* **2014**, *50*, 15718-15721.

(46) Zhu, J.; Lin, Z.; Marder, T. B. *Inorg. Chem*. **2005**, *44*, 9384-9390.

(47) Iverson, C. N.; Smith, M. R. *J. Am. Chem. Soc*. **1995**, *117*, 4403-4404.

(48) Sakaki, S.; Kai, S.; Sugimoto, M. *Organometallics* **1999**, *18*, 4825-4837.

(49) Lin, T.-P.; Peters, J. C. *J. Am. Chem. Soc*. **2014**, *136*, 13672-13683.

(50) Johansson, R.; Wendt, O. F. *Organometallics* **2007**, *26*, 2426-2430.

(51) Schmeier, T. J.; Dobereiner, G. E.; Crabtree, R. H.; Hazari, N. *J. Am. Chem. Soc*. **2011**, *133*, 9274-9277.

(52) Schmeier, T. J.; Nova, A.; Hazari, N.; Maseras, F. *Chem. Eur. J*. **2012**, *18*, 6915-6927.

(53) Ostapowicz, T. G.; Hölscher, M.; Leitner, W. *Chem. Eur. J*. **2011**, *17*, 10329-10338.

(54) Suh, H. W.; Schmeier, T. J.; Hazari, N.; Kemp, R. A.; Takase, M. K. *Organometallics* **2012**, *31*, 8225-8236.

(55) Rios, P.; Curado, N.; Lopez-Serrano, J.; Rodriguez, A. *ChemCommun* **2016**, *52*, 2114-2117.

(56) Hohenberg, P.; Kohn, W. *Phys. Rev*. **1964***, 136*, B864-B871.

(57) Kohn, W.; Sham, L. *Phys. Rev*. **1965**, *140*, A1133-A1138.

(58) Gaussian 09, Revision D.01, Frisch, M. J.; Trucks, G. W.; Schlegel, H. B.; Scuseria, G. E.; Robb, M. A.; Cheeseman, J. R.; Scalmani, G.; Barone, V.; Mennucci, B.; Petersson, G. A.; Nakatsuji, H.; Caricato, M.; Li, X.; Hratchian, H. P.; Izmaylov, A. F.; Bloino, J.; Zheng, G.; Sonnenberg, J. L.; Hada, M.; Ehara, M.; Toyota, K.; Fukuda, R.; Hasegawa, J.; Ishida, M.; Nakajima, T.; Honda, Y.; Kitao, O.; Nakai, H.; Vreven, T.; Montgomery Jr., J. A.; Peralta, J. E.;

Ogliaro, F.; Bearpark, M.; Heyd, J. J.; Brothers, E.; Kudin, K. N.; Staroverov, V. N.; Keith, T.; Kobayashi, R.; Normand, J.; Raghavachari, K.; Rendell, A.; Burant, J. C.; Iyengar, S. S.; Tomasi, J.; Cossi, M.; Rega, N.; Millam, J. M.; Klene, M.; Knox, J. E.; Cross, J. B.; Bakken, V.; Adamo, C.; Jaramillo, J.; Gomperts, R.; Stratmann, R. E.; Yazyev, O.; Austin, A. J.; Cammi, R.; Pomelli, C.; Ochterski, J. W.; Martin, R. L.; Morokuma, K.; Zakrzewski, V. G.; Voth, G. A.; Salvador, P.; Dannenberg, J. J.; Dapprich, S.; Daniels, A. D.; Farkas, O.; Foresman, J. B.; Ortiz, J. V.; Cioslowski, J.; Fox, D. J. In Gaussian, Inc. Wallingford CT, **2013**.

(59) Adamo, C.; Barone, V. *J. Chem. Phys*. **1999**, *110*, 6158-6170.

(60) Dolg, M.; Wedig, U.; Stoll, H.; Preuss, H. *J. Chem. Phys*. **1987**, *86*, 866-872.

(61) Fukui, K. *Acc. Chem. Res*. **1981**, *14*, 363-368.

(62) Marenich, A. V.; Cramer, C. J.; Truhlar, D. G. *J. Phys. Chem. B* **2009**, *113*, 6378-6396.

(63) Grimme, S.; Antony, J.; Ehrlich, S.; Krieg, H. *J. Chem. Phys*. **2010**, *132*, 154104.

(64) Miloserdov, F. M.; McKay, D.; Muñoz, B. K.; Samouei, H.; Macgregor, S. A.; Grushin, V. V. *Angew. Chem. Int. Ed*. **2015**, *54*, 8466-8470.

(65) Miloserdov, F. M.; McMullin, C. L.; Belmonte, M. M. n.; Benet-Buchholz, J.; Bakhmutov, V. I.; Macgregor, S. A.; Grushin, V. V. *Organometallics* **2014**, *33*, 736-752.

(66) Watson, L.; Eisenstein, O. *J. Chem. Ed*. **2002**, *7*9, 1269.

(67) Han, L.-L.; Li, S.-J.; Fang, D.-C. *Phys. Chem. Chem. Phys*. **2016**, *18*, 6182-6190.

(68) Mammen, M.; Shakhnovich, E. I.; Deutch, J. M.; Whitesides, G. M. *J. Org. Chem*. **1998**, *63*, 3821-3830.

(69) Martin, R. L.; Hay, P. J.; Pratt, L. R. *J. Phys. Chem. A* **1998**, *102*, 3565-3573.

(70) Wertz, D. H. *J. Am. Chem. Soc*. **1980**, *102*, 5316-5322.

(71) Abraham, M. H. *J. Am. Chem. Soc.* 1981, 103, 6742-6744.

(72) Deubel, D. V. *J. Am. Chem. Soc*. **2008**, *130*, 665-675.

(73) Kua, J.; Krizner, H. E.; De Haan, D. O. *J. Phys. Chem. A* **2011**, *115*, 1667-1675.

(74) Courtemanche, M.-A.; Pulis, A. P.; Rochette, E.; Legare, M.-A.; Stephan, D. W.; Fontaine, F.-G. *ChemCommun* **2015**, *51*, 9797-9800.

(75) Schmeier, T. J.; Hazari, N.; Incarvito, C. D.; Raskatov, J. A. *ChemCommun*. **2011**, *47*, 1824-1826.

(76) Chakraborty, S.; Patel, Y. J.; Krause, J. A.; Guan, H. *Polyhedron* **2012**, *32*, 30-34.

(77) Suh, H.-W.; Guard, L. M.; Hazari, N. *Polyhedron* **2014**, *84*, 37-43.

(78) Very small amounts of silylformate were detected by NMR. See reference 55 for details.

(79) Suh, H.-W.; Guard, L. M.; Hazari, N. *Chem. Sci.* ***2014***, *5*, 3859-3872.

(80) Berkefeld, A.; Piers, W. E.; Parvez, M. *J. Am. Chem. Soc*. **2010**, *132*, 10660-10661.

(81) Peuser, I.; Neu, R. C.; Zhao, X.; Ulrich, M.; Schirmer, B.; Tannert, J. A.; Kehr, G.; Fröhlich, R.; Grimme, S.; Erker, G.; Stephan, D. W. *Chem. Eur. J.* **2011**, *17*, 9640-9650.

(82) Hydrosilylation of **3**, without $B(C_6F_5)_3$, was calculated to have an energy barrier comparable to the first step of the two pathways described in the text, *i.e*. the Lewis acid does not

facilitate hydrosilylation. However, the stoichiometric reaction of **3** with Et_3SiH yields decomposition of the former above 40ºC and this route was not further considered.

(83) Lin, T.-P.; Peters, J. C. *J. Am. Chem. Soc*. **2013**, *135*, 15310-15313.

(84) Wen, M.; Huang, F.; Lu, G.; Wang, Z.-X. *Inorg. Chem*. **2013**, *52*, 12098-12107.

(85) Houghton, A. Y.; Hurmalainen, J.; Mansikkamäki, A.; Piers, W. E.; Tuononen, H. M. *Nat. Chem*. **2014**, *6*, 983-988.

(86) Parks, D. J.; Piers, W. E. *J. Am. Chem. Soc*. **1996**, *118*, 9440-9441.

(87) Rendler, S.; Oestreich, M. *Angew. Chem. Int. Ed*. **2008**, *47*, 5997-6000.

(88) Berkefeld, A.; Piers, W. E.; Parvez, M.; Castro, L.; Maron, L.; Eisenstein, O. *J. Am. Chem. Soc.* **2012**, *134*, 10843-10851.

(89) Voss, T.; Mahdi, T.; Otten, E.; Fröhlich, R.; Kehr, G.; Stephan, D. W.; Erker, G. *Organometallics* **2012**, *31*, 2367-2378.

(90) Cummings, S. A.; Iimura, M.; Harlan, C. J.; Kwaan, R. J.; Trieu, I. V.; Norton, J. R.; Bridgewater, B. M.; Jäkle, F.; Sundararaman, A.; Tilset, M. *Organometallics* **2006**, *25*, 1565-1568.

(91) Castro-Rodriguez, I.; Nakai, H.; Zakharov, L. N.; Rheingold, A. L.; Meyer, K. *Science* **2004**, *305*, 1757-1759.

(92) Chen, J.; Falivene, L.; Caporaso, L.; Cavallo, L.; Chen, E. Y. X. *J. Am. Chem. Soc*. **2016**, *138*, 5321-5333.

(93) Sakata, K.; Fujimoto, H. *J. Org. Chem*. **2013**, *78*, 12505-12512.

TOC GRAPHIC

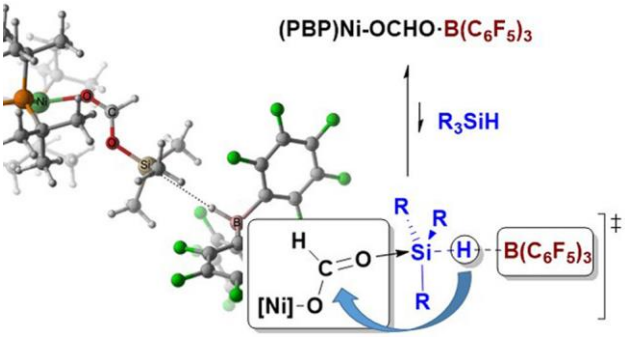

A mechanism for the selective hydrosilylation of CO_2 to the aldehyde level by a bisphosphinoboryl (PBP) nickel complex is described. The results reveal the origin of the selectivity and the roles of $[(PBP)Ni]^+$ and $[HB(C_6F_5)_3]^-$ in the sequence of hydride and silylium (R_3Si^+) transfers to CO_2 and formate ligands that lead to reduction.